Original Article

MOLECULAR METABOLISM

Upregulated ethanolamine phospholipid synthesis via selenoprotein I is required for effective metabolic reprogramming during T cell activation

Chi Ma [1], FuKun W. Hoffmann [1], Michael P. Marciel [1], Kathleen E. Page [2], Melodie A. Williams-Aduja [2], Ellis N.L. Akana [2], Greg S. Gojanovich [1], Mariana Gerschenson [1], Johann Urschitz [3], Stefan Moisyadi [3], Vedbar S. Khadka [4], Sharon Rozovsky [5], Youping Deng [4], F. David Horgen [2], Peter R. Hoffmann [1,*]

ABSTRACT

Objective: T cell activation triggers metabolic reprogramming to meet increased demands for energy and metabolites required for cellular proliferation. Ethanolamine phospholipid synthesis has emerged as a regulator of metabolic shifts in stem cells and cancer cells, which led us to investigate its potential role during T cell activation.

Methods: As selenoprotein I (SELENOI) is an enzyme participating in two metabolic pathways for the synthesis of phosphatidylethanolamine (PE) and plasmenyl PE, we generated SELENOI-deficient mouse models to determine loss-of-function effects on metabolic reprogramming during T cell activation. Ex vivo and in vivo assays were carried out along with metabolomic, transcriptomic, and protein analyses to determine the role of SELENOI and the ethanolamine phospholipids synthesized by this enzyme in cell signaling and metabolic pathways that promote T cell activation and proliferation.

Results: SELENOI knockout (KO) in mouse T cells led to reduced de novo synthesis of PE and plasmenyl PE during activation and impaired proliferation. SELENOI KO did not affect T cell receptor signaling, but reduced activation of the metabolic sensor AMPK. AMPK was inhibited by high [ATP], consistent with results showing SELENOI KO causing ATP accumulation, along with disrupted metabolic pathways and reduced glycosylphosphatidylinositol (GPI) anchor synthesis/attachment

Conclusions: T cell activation upregulates SELENOI-dependent PE and plasmenyl PE synthesis as a key component of metabolic reprogramming and proliferation.

Keywords Selenium; Selenoprotein; Phosphatidylethanolamine; Ethanolamine phosphotransferase; Metabolic sensing; AMPK; Glycolysis

1. INTRODUCTION

T cell lymphocytes play a central role in coordinating immune responses and carrying out effector functions to eliminate pathogens or cancer cells. T cells are activated through cell surface T cell receptors (TCRs) with co-receptors such as CD28, which together trigger cellular proliferation [1]. Sufficient TCR signal strength is critical for optimal activation through a complex signaling network that leads to upregulated transcriptional programs for T cell growth factors such as IL-2 along with its high affinity receptor chain, CD25 [2–4]. In addition, TCR-induced activation promotes cell cycle progression by triggering metabolic reprogramming to meet demands for energy and intermediate molecules required for the biosynthesis of proteins, nucleic acids, and lipids [5,6]. This metabolic reprogramming includes changes in glycolysis, nucleic acid, and fatty acid metabolism, and mitochondrial respiration that are regulated by signals initiated at the T cell surface and further modulated through sensing pathways that provide feedback on metabolite excesses or deficiencies.

One example of an important sensor of energy and metabolites in T cells is AMP-activated protein kinase (AMPK) [7]. AMPK is a

[1]Department of Cell and Molecular Biology, John A. Burns School of Medicine, University of Hawaii, Honolulu, HI 96813, USA [2]Department of Natural Sciences, Hawaii Pacific University, Kaneohe, HI 96744, USA [3]Department of Anatomy, Physiology and Biochemistry, John A. Burns School of Medicine, University of Hawaii, Honolulu, HI 96813, USA [4]Department of Quantitative Health Sciences, John A. Burns School of Medicine, University of Hawaii, Honolulu, HI 96813, USA [5]Department of Chemistry and Biochemistry, University of Delaware, Newark, DE 19716, USA

*Corresponding author. John A. Burns School of Medicine, 651 Ilalo Street, Honolulu, HI, 96813 USA. Tel.: 01-808-692-1510. E-mail: peterrh@hawaii.edu (P.R. Hoffmann).

Abbreviations: AAG, 1-alkyl, acylglycerol; AMPK, AMP-activated protein kinase; BUB1, benzimidazoles 1; CEPT1, choline/ethanolamine phosphotransferase 1; CCNE1, cyclin E1; CDP, cytidine 5-diphosphate; DAG, diacylglycerol; DEGs, differentially expressed genes; E2F3, E2F transcription factor 3; ER, endoplasmic reticulum; GPI, glycosylphosphatidylinositol; GPAA1, GPI anchor attachment protein 1; KO, knockout; PPP, pentose phosphate pathway; PE, phosphatidylethanolamine; SELENOI, selenoprotein I; TCR, T cell receptor; WT, wild-type

Received December 9, 2020 • Revision received January 2, 2021 • Accepted January 18, 2021 • Available online 20 January 2021

https://doi.org/10.1016/j.molmet.2021.101170

heterotrimeric complex comprised of a catalytic α subunit with serine (Ser)/threonine (Thr) kinase activity, which combines with β and γ subunits that regulate its activation and substrate specificity. AMPK activity is stimulated by phosphorylation of the catalytic a subunit at Thr172, and phosphatase cleavage at this residue is blocked by AMP and ADP binding at that residue. In contrast, an abundance of ATP displaces AMP or ADP to promote AMPK dephosphorylation, reducing its activity [8]. TCR-induced signaling leads to rapid increases in ATP that is subsequently degraded into ADP/AMP as an energy source during anabolic reactions required for cell cycle progression. Defects in generating ATP or utilizing it to fuel biomolecule synthesis during T cell activation are sensed by AMPK and may lead to impaired cell cycle progression [9]. Determining how different synthesis pathways feed into metabolic reprogramming, how energy production and expenditure are balanced, and how disruptions in these processes are sensed is critical for understanding effective T cell activation and optimal proliferation.

Recent investigations into phospholipid synthesis pathways revealed that ethanolamine phospholipids are particularly important for metabolic reprogramming in pluripotent stem cells [10] and proliferating tumor cells [11]. This raises the question of whether this class of phospholipids may also be involved in metabolic reprogramming of activated T cells that is required for proliferation. Selenoprotein I (SELENOI, aka ethanolamine phosphotransferase-1) is a member of the selenoprotein family, with many members exhibiting oxidoreductase enzymatic activity [12]. SELENOI is not an oxidoreductase enzyme, but instead an ethanolamine phosphotransferase involved in the synthesis of two different ethanolamine phospholipids: phosphatidylethanolmine (PE) and plasmenyl PE [13,14]. The former is synthesized through the Kennedy pathway at the cytosol/endoplasmic reticulum (ER) interface, with SELENOI catalyzing the final reaction between cytidine 5-diphosphate (CDP)-ethanolamine and 1,2-diacylglycerol (DAG) to generate PE [15]. Plasmenyl PE is synthesized through a separate pathway beginning in the peroxisomes (reactions 1–3) and finishing in the ER membrane (reactions 4–7). SELENOI catalyzes the sixth reaction involving attachment of the phosphoethanolamine head group from CDP-ethanolamine to 1-alkyl-2-acylglycerol (AAG) to generate plasmenyl PE [16]. PE and plasmenyl PE species serve structural functions in cellular membranes, but possible roles in signaling pathways and metabolic regulation are beginning to emerge [10,17].

It is unclear whether SELENOI-dependent ethanolamine phospholipid synthesis is affected by T cell activation or how SELENOI may participate in phospholipid reprogramming to regulate T cell activation and proliferation. The data presented herein demonstrate that T cell activation leads to increased levels of SELENOI enzyme along with PE and plasmenyl PE. SELENOI deficiency in mouse T cells reduced de novo synthesis of PE and plasmenyl PE as well as proliferation. T cell activation in SELENOI knockout (KO) resulted in an accumulation of ATP and decreased AMPK activation, disrupted metabolic reprograming, and reduced cell cycle progression and pro-growth pathways. These data provide new insight into how activated T cells rely on increased SELENOI-dependent PE and plasmenyl PE synthesis, which play an important role in metabolic reprogramming required for cellular proliferation.

2. MATERIALS AND METHODS

2.1. Mice

A conditional SELENOI knockout mouse model was used to generate a SELENOI$^{fl/fl}$ colony as previously described [18]. *Lck*-Cre (distal promoter) mice were purchased from Jackson Laboratories and bred with SELENOI$^{fl/fl}$ mice. Because the *lck*-Cre system excises floxed alleles late in T cell development in the thymus [19], we analyzed our SELENOI T cell-specific KO mice for levels of CD4$^+$ and CD8$^+$ T cells in the thymus, spleen, and lymph nodes to confirm that these lymphoid tissues were populated with adequate numbers of mature T cells. Results confirmed KO by real-time PCR, Western blotting, and flow cytometry showed similar levels of these T cells in these lymphoid tissues when comparing the SELENOI T cell-specific KO mice and three different controls and confirmed SELENOI KO in splenic T cells (Supplemental Figure 1). The UH Manoa Transgenic Core used a *piggyBac* transposon-based plasmid to generate a stable doxycycline (DOX)-inducible SELENOI KD mouse line. Prior to plasmid construction, the Broad Institute's Gene Perturbation website (https://www.broadinstitute.org/genetic-perturbation-platform) was used to identify five different shRNAs with SELENOI-specific target sequences. After testing a panel of these shRNAs (Horizon Discovery, Inc.) in HEK293 cells, we identified the most effective sequence as ATC AGA TAC AGT AAG AGC C and used it for our plasmids (Supplemental Figure 4). The basis for the final plasmids used in te-PNI transgenesis was a commercially obtained TET-ON micro-RNA (miR30) adapted shRNA vector targeting the RNA of mouse glucose transporter 1 (Glut1; V3THS_321626, Open Biosystems). This V3THS_321626 plasmid encoded turboRFP under a TRE-3G promoter, with reverse tetracycline-controlled transactivator 3 (rTTA3) driven by a ubiquitin C gene (*ubc*) promoter. ShRNAmir was situated in the 3′UTR of turboRFP. We replaced turboRFP with the luciferase reporter gene to enable the in vivo assessment of transgene expression. The *ubc* promoter was replaced with the stronger *cmv* promoter to enhance the expression of luciferase and shRNAmir. We exchanged the shRNA target sequence of Glut1 with that of SELENOI. These steps were performed using restriction digestion and ligation cloning. The transgene was then cloned into a pENTR1A vector (Thermo Fisher Scientific) to facilitate the final step, the recombination of this SELENOI KD pENTR1A vector with our pmhyGENIE-3 *piggyBac* vector to generate the final construct, and transgenesis of oocytes was performed as previously described [20,21]. The KO and DOX-inducible KD T cells were confirmed by western blotting (Supplemental Figures 1 and 4). Experiments using the mice included age/sex matched males and females 8–12 weeks of age. The animal protocols were approved by the University of Hawaii's Institutional Animal Care and Use Committee.

2.2. Mouse genotyping and phenotyping

To genotype and detect the floxed SELENOI alleles in DNA extracted from mouse tails, PCR was carried out for the 3′ *loxp* site using fwd 5′-GTC TGT GTG AGG TTG TTG GAT CTC C-3′ and rev 5′-GCA TAT AGG TGT AGA GAA AAT AGG TAT GCA AAC C-3′. For the 5′ *loxp* site, the following primers were used: fwd 5′-GCA CTA GAG AGC CTA TAA ACC AAG ACT GC-3′ and rev 5′-CCA GAG GAT GTG AGC TTG GCG-3′. The PCR products exhibited a 34-nucleotide difference with and without *loxp* sites. To detect non-excised and excised alleles, respectively, the following PCR primers were used: fwd 5′-TTC CAG GGG TGC TTA GGT CT-3′ and rev 5′-AGA TCT GCC TGC CTA TGT GC-3′ (544 bp product), fwd 5′-TGT GAG TGT GCT GGG TTA GG-3′, and rev 5′-GGG TGG CAG ATG GGT ACA TAA-3′ (450 bp product). The PCR conditions were as follows: 94 °C for 2 min; 10 cycles: 94 °C for 20 s, 65 °C for 15 s, and 68 °C for 10 s; 28 cycles: 94 °C for 15 s, 60 °C for 15 s, and 72 °C for 20 s; and 72 °C for 2 min. To genotype the SELENOI DOX-inducible mice, the following primers were used: EPT1 fwd 5′-AGA TCG CCG TGT AAT TCT GG-3′ and EPT1 rev 5′-CAG GGT AGG CTG CTC AAC TC-3′.

2.3. T cell isolation, activation, and imaging

Spleens and lymph nodes (inguinal and axillary) excised from euthanized mice were homogenized into a single cell suspension followed by $CD3^+$ T cell isolation using a Mouse Pan T cell isolation kit (Miltenyi Biotec), with isolated cells counted using a Millipore Scepter. For human T cells, whole blood was obtained from healthy volunteers as approved by the University of Hawaii's institutional review board, and a T cell enrichment column (R&D Systems) was used for T cell isolation. Mouse and human T cells were activated through the T cell receptor (TCR) in 96-well plates precoated with BioLegend anti-CD3 (clones 145-2C11 and OKT3; 10 μg/mL) plus anti-CD28 (clones 37.51 and CD28.2; 1 μg/mL). Cells were incubated for different periods in RPMI-1640 media containing 10% Seradigm 1500-500 FBS (VWR). In some cases, the expression of SELENOI shRNA was induced in vivo by i. p. injecting DOX at 5 μg/g per day for 2 d prior to spleen/lymph node harvest. Ex vivo T cells from these mice were cultured in complete media containing 2 μg/mL of DOX for continued KD of SELENOI. Images of proliferating T cells were captured on a Zeiss Axiovert 200M attached to a Zeiss LSM 5 Pascal imaging system.

2.4. Flow cytometry evaluation of lymphoid tissues and T cells

For thymus, lymph node, and spleen tissues, single cell suspensions were preincubated with anti-CD16/32 for 15 min followed by antibody stains. BD Pharmingen antibodies used at concentrations recommended by the vendor included FITC-anti-CD8 (clone 53—5.8), PE-anti-CD44 (clone IM7), and PE/Cy7-anti-CD16/32 (clone 2.4G2). BioLegend antibodies included FITC-anti-CD3 (clone 145-2C11), APC-anti-CD4 (clone GK1.5), and APC/Cy7-anti-CD8 (clone 53—5.8). Cell Signaling antibodies included PE-anti-p-ERK1/2 (Thr202, Thr204, and clone 6B8B69), PE-anti-p-AKT (Ser473; clone D9E), and PE-anti-p-AKT (Thr308; clone D25E6). Dead cells were detected with BV421 viable dye (Invitrogen). Flow cytometry was performed using a BD LSRFortessa cell analyzer and the data were analyzed using FlowJo software.

2.5. Cell proliferation assays and in vivo antigen challenge

Mouse primary $CD3^+$ T cells were negatively purified using a Mouse Pan T cell isolation kit (Miltenyi), and 10^6 cells were resuspended in 1 mL of cold PBS. The cells were loaded with 1 μL of 5 μM CellTrace CSFE (Thermo Fisher Scientific) in DMSO and incubated at room temperature protected from light for 20 min. Complete culture medium (4 mL) was added to the cells and incubated for 5 min to remove excess CSFE. The cells were centrifuged for 5 min at $300\times g$ at 4 °C, the supernatant was removed by decanting, and the cell pellets were resuspended with 1 mL of complete medium. The cells (2×10^5/200 μL) were plated in each well in a 96-well plate precoated with anti-CD3 antibody (10 μg/mL) and anti-CD28 (1 μg/mL) (both from BioLegend). Cells were cultured for 72 h and analyzed using a BD LSRFortessa cell analyzer and data analyzed using FlowJo software. In some cases, dorsomorphin (Sigma) was added at different concentrations at the time of plating (day 0) and on days 1 and 2 followed by harvest and analysis on day 3. The Proliferation Index was calculated as the total number of divisions divided by the number of cells that underwent division. Because the Proliferation Index only considered the cells that underwent at least one division, only the responding cells were reflected in this value. Our previously described protocol for peptide antigen injections and antigen-specific T cell analysis [22] was followed with modifications. Lymphocytic choriomeningitis virus (LCMV) peptide was purchased, MHC-I restricted antigen gp33-41 (KAVYNFATM; AnaSpec, Inc.). Mice were s. c. injected with 50 μL of complete Freund's adjuvant (Sigma) emulsified with gp33-41 peptide (20 μg in 50 μL of PBS) on day 0 and boosted on day 10 with emulsified incomplete Freund's adjuvant plus peptide at the same concentration. On day 14, the mice were sacrificed and their spleen cells were analyzed by flow cytometry following the tetramer staining protocol recommended by the NIH Tetramer Core Facility. In brief, the APC-conjugated tetramer (H-$2D^b$ KAVYNFATM-APC) obtained from the NIH Tetramer Facility was dissolved in an aqueous buffer containing 0.5 mM of EDTA, 0.2% BSA, 10 mM of Tris—HCl (pH 8.0), and 150 mM of NaCl. Tetramer (10 μL) was added to 150 μL of cell suspension via vortexing. The samples were incubated at room temperature for 1 h. For the final 30 min, a cocktail of antibodies was added at the manufacturer's recommended concentrations. Red blood cells were lysed using RBC lysis reagent (MBL International) as recommended and the cells washed with 1 mL of PBS. Following centrifugation at $150\times g$ for 5 min, the media was aspirated, and the cells were resuspended in FACS buffer. Flow cytometry was performed using a BD LSRFortessa cell analyzer and the data were analyzed using FlowJo software.

2.6. Western blotting, real-time PCR, and enzyme assays

Cell lysates were prepared as previously described [23], and 30 μg of total protein was loaded per well on a 20% Criterion polyacrylamide gel (Bio-Rad), transferred to nitrocellulose (VWR), and incubated with blocking buffer (Millipore). Primary antibodies were added at a 1:1000 final dilution. Secondary antibodies (Li-Cor) were added at 1:500—1:1000 final dilution, and fluorescent signals were detected using a Li-Cor Odyssey infrared imaging system. Primary antibodies included anti-SELENOI (ProMab), anti-AKT/anti-p-AKT(Ser405), anti-Rictor/anti-p-Rictor, anti-AMPK/anti-p-AMPK (all from Cell Signaling), and anti-β-actin (Santa Cruz). Real-time PCR was carried out on a LightCycler 480 (Roche) using a SYBR Green kit (Qiagen) and primers as previously described [24,25]. Ethanolamine phosphotransferase activity was determined using whole cell lysates of kidney tissue lysed in 20 mM of Tris—HCl at pH 8.0 with a protease inhibitor cocktail (Carbiochem) in a water bath sonicator for 1 min. The protein content of the lysate was determined by a Bradford assay and normalized to 4 mg/mL. The reaction mixture (25 μL) contained 50 mM of Tris—HCl buffer, pH 8.0, 5 mM of MnCl2, 1 mM of EGTA, 0.5 mM of 1-palmitoyl-2 (dipyrrometheneboron difluoride) undecanoyl-sn-glycerol (Avanti Lipids), 0.002% (w/v) Tween 20, 50 μg of cell lysate, and 20 μM of CDP-ethanolamine (Toronto Research Chemicals Inc., Toronto, ON, Canada). After incubation at 37 °C for 10 min, the reaction was stopped by adding 60 μL of chloroform methanol (1:1 v/v) followed by 30 μL of 0.9% KCl. After centrifugation at 8,000 g for 5 min, the organic phase was applied to precoated silica gel 60 thin layer chromatography (TLC) plates (Merck, Darmstadt, Germany), which were then developed with chloroform methanol (1:1 v/v). TopFluor-conjugated phospholipids were analyzed using a Gel Logic 200 Imaging System (Kodak) and quantified using ImageJ version 1.46r. An ATP determination kit from Invitrogen was used to measure the ATP in the cells.

2.7. Microarrays

Freshly isolated mouse T cells were plated in 6-well plates (6×10^6 cells per well) and stimulated using plate-bound anti-CD3/CD28 as previously described for 20 h followed by RNA isolation using an EZNA Total RNA kit (Omega Bio-tek, Inc). The RNA integrity was validated on an Agilent 2100 Bioanalyzer using RNA Nano chip. For gene expression profiling, 100 ng of total RNA was used for downstream processing using the GeneChip Whole Transcript Expression protocol followed by hybridization to Clariom S array chips (Affymetrix). Subsequently, the arrays were washed, stained, and scanned using a GeneChip Fluidics Station 450 and GeneChip Scanner (Affymetrix). Generated CEL files were normalized using the SST-RMA-GENE-FULL algorithm in the

Affymetrix GeneChip Expression console software. Raw CEL files generated from Clarion S human microarrays were preprocessed in R version 3.6.1 using data normalization via the Robust Multi-Array Average (RMA) approach. Genes with Exp2 (default) transformed fold changes greater or less than 2 and a Benjamini and Hochberg FDR-adjusted p value < 0.05 were considered differentially expressed in the KO with respect to WT. The CEL files were processed and analyzed using Transcriptome Analysis Console (TAC) 4.0 software from Thermo Fisher Scientific. Genes with a fold change greater than 2 or less than -2 and a p value < 0.05 were considered differentially expressed in the KO with respect to WT. WikiPathways analysis integrated within TAC 4.0 was also used to identify significant biological pathways.

2.8. Flow cytometry for GPI-anchored proteins and PE analyses

Isolated mouse T cells were TCR-stimulated as previously described for 1–3 d. For GPI-anchored proteins, antibodies included PE-anti-CD45.2, FITC-anti-Sca-1, PE-anti-CD109, APC-anti-CD24, PE/Cy5-anti-CD44, APC-anti-CD90, PE-anti-CD59a, PE/Cy7-anti-CD37, and PE/Cy5-anti-CD48 (all from BioLegend). For PE staining, cells (0.5×10^6) were fixed with 200 μL of fixation buffer (BioLegend) in a 96-well plate in the dark for 20 min at room temperature, then centrifuged at $400\times g$ for 5 min and the supernatant was discarded. The cells were resuspended and permeabilized in 250 μL of Intracellular Staining Perm Wash Buffer (BioLegend) and centrifuged at $400\times g$ for 10 min. The permeabilization steps were repeated twice. The cells were resuspended and stained in 100 μL of Perm Wash Buffer with 0.5 μM of duramycin-LC-fluorescein or duramycin-LC-Cy5 (Molecular Targeting Technologies). As a control, 1 μM of BSA-FITC (Nanocs, Inc.) was added to the cells for 30 min in the dark at room temperature. After staining, the cells were washed twice with 250 μL of Perm Wash Buffer or TES buffer and centrifuged at $400\times g$ for 5 min. The cells were then resuspended in 150 μL of Cell Staining Buffer (BioLegend) and analyzed together with non-stained controls using a BD LSRFortessa cell analyzer, and the data were analyzed using FlowJo software (BD Biosciences).

2.9. Lipid profiling, metabolomics, and live cell energy measurements

LCMS was used to measure membrane lipid species in cell pellets. The cell pellets ($5–15 \times 10^6$) were enumerated using a Millipore Scepter and the accuracy was verified by comparing the DNA content using CyQuant (Thermo Fisher Scientific). Lipids were extracted from the pellets using one of two established methods [26,27]. The cell pellets were stored at -80 °C until use and then extracted with methyl *tert*-butyl ether/methanol/water (10:3:2.5 v/v/v) or chloroform/methanol/water (8:4:3) with vortexing and sonication. After adding internal synthetic lipid standards (PE 15:0,15:0 and PC 15:0,15:0; Avanti Lipids, Alabaster, AL, USA) and incubating for 40–60 min, the samples were then centrifuged at $1{,}000\times g$ for 10 min at 5 °C and the organic phase was removed, concentrated under a stream of N_2, and dried to completion under a high vacuum. Prior to the LCMS analysis, the dried extracts were reconstituted with isopropanol. Calibration curves were constructed for synthetic lipids by serial quarter-log dilutions in isopropanol. Prior to the LCMS analysis, the dried extracts were reconstituted with isopropanol. Calibration curves were constructed for antipolar lipid synthetic lipid standards PE(15:0,15:0) and PC(15:0,15:0) by serial quarter-log dilutions in isopropanol. The extracts were spiked with the same non-natural glycerophospholipid standards to determine the extraction efficiencies. The protein content was measured using a bicinchoninic acid assay (BCA assay; Bio-Rad). Electrospray ionization LCMS analysis was performed on an Agilent (Santa Clara, CA, USA) 6530 Quadrapole-Time-of-Flight (QTOF) mass spectrometer. Reversed phase (Waters Xbridge column, 2.1 mm $\times$ 150 mm, particle size of 2.5 μm) LC conditions were adapted from Ulmer et al. [28]. The QTOF parameters were: positive mode, gas temperature of 350 °C, N_2 gas flow at 8 L/min, nebulizer at 35 psi, VCap at 3500 V, fragmentor at 140 V, and MS mass range of 100–1700 Da. The samples were measured by MS, while the pooled samples were measured by untargeted MS/MS (collision energies at 10, 20, and 40). Glycerophospholipid peaks were identified by MS/MS experiments and measured by integrating MH^+ extracted ion chromatogram peaks (Agilent MassHunter Quantitative Analysis version 10.0) and the mass of each lipid was determined semi-quantitatively using the calibration curve from the corresponding (PE or PC) standard. For metabolic labeling experiments, ethanolamine-$^{13}C_2$–HCl was purchased from Sigma and added to culture media during an 18 h TCR stimulation at a concentration of 45 mM, and analyzed by LCMS as previously described. The cell pellets (15×10^6) were processed by Metabolon (Morrisville, NC, USA) using Metabolon's Precision Metabolomics LCMS global metabolomics service. Datasets comprised a total of 370 compounds of known identity were used to quantify metabolites, and the data were normalized to the Bradford protein concentration, followed by log transformation and imputation of missing values, if any, with the minimum observed value for each compound. The T cell oxygen consumption rate (OCR) was assessed using a Mito Stress test and Seahorse XFe96 (Agilent Technologies, Santa Clara, CA, USA), which used high-throughput oximetry to simultaneously measure the OCR and extracellular acidification (ECAR) rates as previously described [29]. Reagents were added through injection ports every 30 min and included anti-CD3/28 Mouse Expansion Dynabeads (1:1 bead/cell ratio; Thermo Fisher Scientific), and the final concentrations of reagents included in a Seahorse XF Cell Mito Stress Test kit from Agilent: oligomycin (1 mM), carbonyl cyanide-4 (trifluoromethoxy) phenylhydrazone (FCCP) (1.5 mM), and rotenone (100 nM) together with antimycin (1 mM).

2.10. Statistical analyses

Comparison of two means was carried out via an unpaired Student's t test using GraphPad Prism version 4.0. In assays involving three or more groups, one-way ANOVA was used to analyze groups with Tukey's post-test used to compare the means of each group. All of the comparisons were considered significant at $p < 0.05$. GraphPad Prism was also used to generate standard curves with regression analyses from which values were calculated for the sample measurements. Welch's two-sample t test was used in metabolomics to test whether two unknown means were different from two independent populations.

3. RESULTS

3.1. SELENOI, PE, and plasmenyl PE levels increased upon T cell activation

TCR-induced activation alters metabolism and causes increased cell sizes to prepare T cells for proliferation [6,30]. We evaluated how T cell activation affects levels of SELENOI, which participates in two synthesis pathways for the ethanolamine phospholipids, PE and plasmenyl PE. Anti-CD3/CD28 activation of purified mouse T cells led to an expected increase in cell sizes as well as higher levels of PEs, plasmenyl PEs, and phosphatidylcholines (PCs; included as a comparison phospholipid) (Figure 1A–B). Real-time PCR analysis of the mouse selenoprotein transcriptome showed that SELENOI was among the most upregulated selenoprotein mRNAs in activated T cells compared to

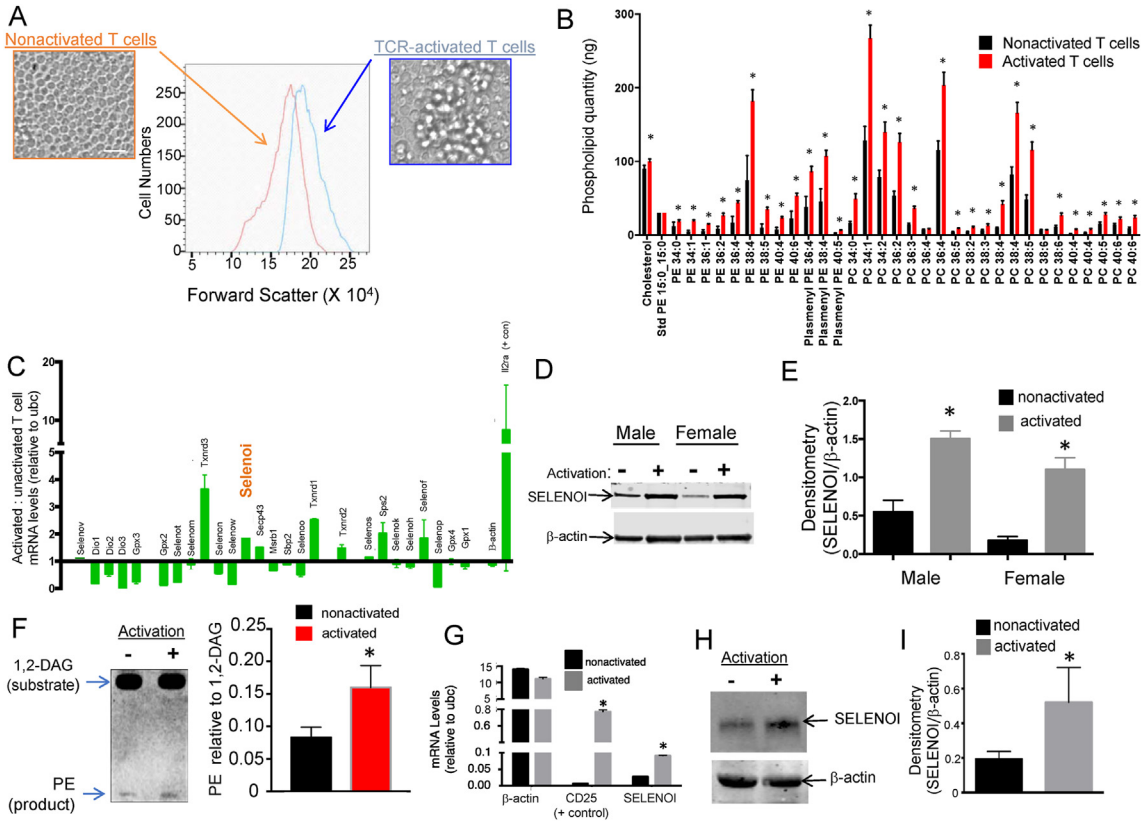

Figure 1: T cell activation led to increased cell size and phospholipid levels as well as upregulated SELENOI. $CD3^+$ T cells purified from mouse spleens were unstimulated or activated with anti-CD3/CD28 for 18 h. (A) Activated T cells showed increased sizes (forward scatter) using flow cytometry. Scale bar = 30 mm. (B) LCMS was used to compare levels of different lipid species extracted from T cells (displayed at pmol/10^6 cells) and changes in PEs, plasmenyl PEs, and PCs are shown. (C) Real-time PCR was used to analyze mRNAs for selenoproteins and selenoprotein synthesis factors in unstimulated and activated T cells. Target mRNAs were normalized to housekeeping mRNA (*ubc*), β-actin was included as a comparison control, and il2ra (encodes for CD25) was included as a positive control. (D–E) Representative western blotting and densitometry analysis of SELENOI protein levels in 3 biological replicate experiments showed increases upon activation, and β-actin was used as a loading control. (F) Thin layer chromatography was used to analyze SELENOI activity (left) and the results of three independent experiments showed increases upon T cell activation (right). (G–I) Human T cells isolated from peripheral blood exhibited increases in SELENOI mRNA and protein after 18 h of anti-CD3/CD28 activation. Target mRNAs were normalized to housekeeping mRNA (*ubc*), β-actin was included as a comparison control, and CD25 was included as a positive control. Means of biological replicates (N = 3) were compared using Student's t test and expressed as mean ± SEM with $^*p < 0.05$.

inactivated controls (Figure 1C). This was consistent with a 2-3-fold increase in both SELENOI protein levels and enzyme activity in activated mouse T cells (Figure 1D–F). Similar results were found by real-time PCR and western blotting analyses of activated human T cells (Figure 1G–I). These data suggest that, as an enzyme involved in the synthesis of ethanolamine phospholipids, SELENOI is upregulated in response to TCR stimulation and may be important for optimal T cell activation and proliferation.

3.2. SELENOI deficiency decreased de novo synthesis of PE and plasmenyl PE during T cell activation

We generated T cell-specific SELENOI knockout (KO) mice that exhibited normal T cell populations in their lymphoid tissues (Fig. S1). T cells were isolated from KO and wild-type (WT) mice to determine if SELENOI deficiency would prevent an increase in levels of ethanolamine phospholipids during T cell activation. Using a duramycin peptide probe that binds specifically to PE [31], SELENOI KO T cells were compared to the WT controls by flow cytometry for levels of total PE. We found that increased cell sizes induced by TCR activation did not require SELENOI expression (Figure 2A), and the PE levels were similar between the WT and KO T cells after 18 h of TCR-induced activation (Figure 2B–C). We next evaluated the PE levels as the activated WT and KO T cells underwent successive rounds of division over 3 d of proliferation by combining CFSE and duramycin staining. Again, the PE levels increased equally upon TCR-activation in the WT and SELENOI KO T cells and remained similar throughout proliferation (Figure 2D).

PE can be generated de novo from precursors or converted from other phospholipids such as phosphatidylserine. As a more specific evaluation of the de novo synthesis of the PE and plasmenyl PE during T cell activation, $^{13}C_2$-labeled ethanolamine was added to culture media during the 18 h TCR-induced activation of the WT and KO T cells. Since exogenous ethanolamine feeds directly into the generation of CDP-ethanolamine that serves as a substrate for the synthesis of PE and plasmenyl PE [32,33], addition of $^{13}C_2$-labeled ethanolamine allowed us to conduct LCMS-based measurements of phospholipid species that formed after activation was induced through TCR stimulation. Unlabeled PE and plasmenyl PE species were also measured. The results showed that the $^{13}C_2$-labeled PE (calculated from the detectable $^{13}C_2$-labeled PE species; Figure S2) was ~23% lower in the activated SELENOI KO T cells compared to the WT controls, while the unlabeled PE did not differ (Figure 2E). Consistent with the flow

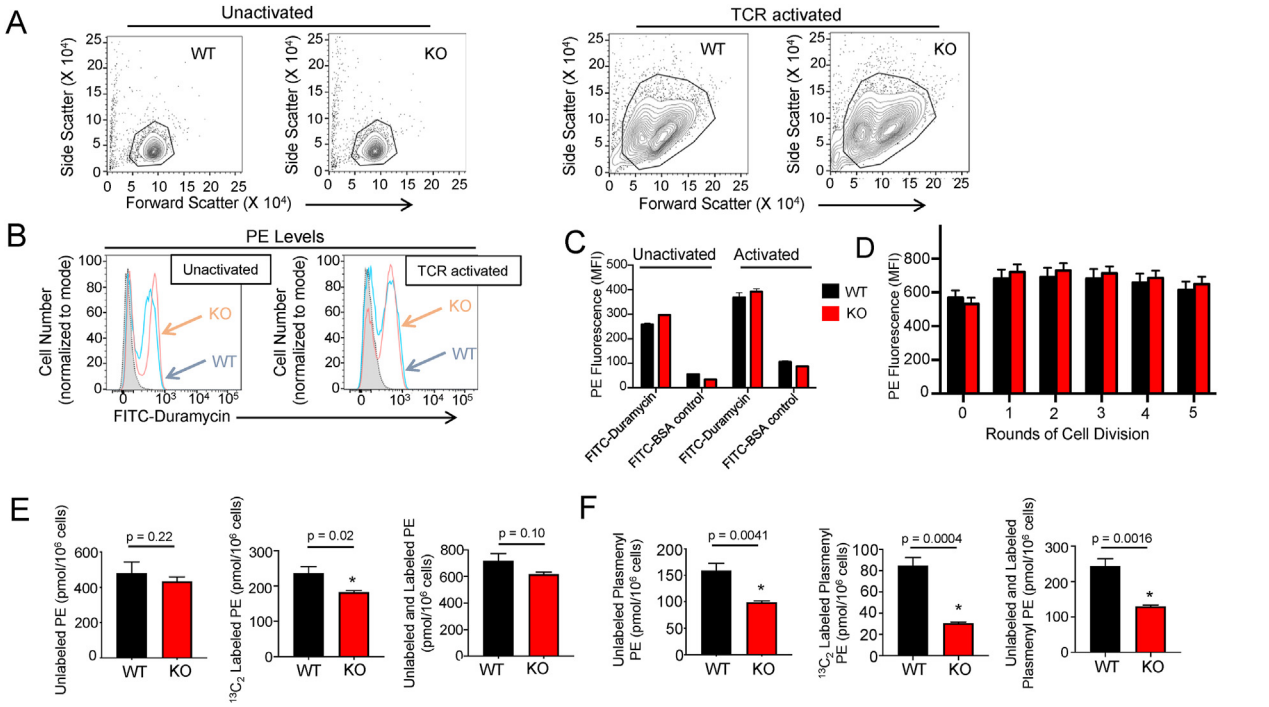

Figure 2: SELENOI deficiency caused decreases in de novo PE and plasmenyl PE synthesis during T cell activation. (A) Flow cytometry analyses of size (forward scatter) vs granularity/size (side scatter) showed equivalent profiles of WT and SELENOI KO T cells. (B–C) An FITC-duramycin probe was used to measure PE levels in inactivated and activated T cells from WT and KO mice. FITC-BSA was used as a negative control probe. (D) Cy5-duramycin combined with CSFE was used to measure PE levels after three days of cell division. (E) T cells were pulsed with $^{13}C_2$-labeled ethanolamine during TCR activation (18 h) and LCMS was used to measure PE species calculated as pmol/10^6 cells (see Figure S2) that were in turn used to calculate the levels of unlabeled and labeled PE. The levels of $^{13}C_2$-labeled PE represent de novo synthesis during the T cell activation period. (F) The same metabolically pulsed T cells were analyzed for the levels of unlabeled and labeled plasmenyl PE. Means of replicates (N = 3) were compared using Student's t test and expressed as mean ± SEM with *p < 0.05.

cytometry data, total PE (unlabeled and labeled) did not significantly differ between the activated WT and KO T cells. As shown in Figure S2, only one $^{13}C_2$-labeled PE species was higher in the activated KO T cells (36:4), while several $^{13}C_2$-labeled PE species were lower and others did not differ. In contrast, all the labeled plasmenyl PE species detected by LCMS decreased in the SELENOI KO T cells compared to the controls (Figure S2), leading to ~64% lower total $^{13}C_2$-labeled plasmenyl PE generated during T cell activation compared to the WT controls (Figure 2F). Unlabeled plasmenyl PE and total plasmenyl PE (unlabeled and labeled) levels also decreased in the KO T cells, but not to the same extent as the labeled plasmenyl PE. Repeated LCMS experiments in the activated WT and KO T cells with no metabolic labeling were conducted to rule out any influence of the $^{13}C_2$ label on phospholipid synthesis. Similar results were obtained showing lower total plasmenyl PE in the activated SELENOI KO T cells compared to the WT controls, but with no significant changes in the total PE (Figure S3). PC was analyzed as a comparison phospholipid with the results showing that the PC species and total PC were similar between the WT and KO, confirming no influence of SELENOI KO on the synthesis of this phospholipid.

The results from these different approaches demonstrated the importance of SELENOI for increased de novo ethanolamine phospholipid synthesis during T cell activation. The plasmenyl PE synthesis pathway is heavily dependent on SELENOI for levels of this phospholipid, particularly plasmenyl PE synthesized during T cell activation. PE synthesis is dependent to a lesser extent, mainly during T activation. T cells appear to be able to compensate for the loss of SELENOI to maintain levels of total PE (unlabeled and labeled), similar to recent studies using HeLa and HEK293 cell lines [34,35].

3.3. SELENOI deficiency reduced the proliferative capacity of activated T cells

Given the SELENOI-dependent increases in de novo PE and plasmenyl PE synthesis observed during T cell activation, we next evaluated how SELENOI KO or doxycycline (DOX)-induced knockdown (KD; Figure S4) may affect T cell proliferation. TCR-induced activation of control T cells (WT or NO DOX) led to cell cultures characterized by clusters of proliferating T cells as previously described [36,37], but proliferating cell clusters were less abundant in the SELENOI KO and DOX-induced KD T cells (Figure 3A–B). CSFE assays revealed that the SELENOI KO T cells commenced cell division that diminished after 1–2 rounds compared to the WT controls that progressed through 5–6 rounds of division, with the Proliferation Index reduced by ~56% in the SELENOI KO T cells (Figure 3C–E). SELENOI KD led to decreased cell division with a Proliferation Index that was reduced by ~22% compared to the controls, suggesting a dosage effect of SELENOI loss of function on proliferation (Figure 3F–H). For the in vivo evaluation of proliferation, we carried out LCMV gp33-41 antigen challenges in the T cell-specific SELENOI KO vs WT controls followed by tetramer staining to analyze antigen-specific T cell levels during the expansion phase. The results showed that SELENOI KO led to ~75% lower antigen-specific T cell levels compared to the controls (Figure 4).

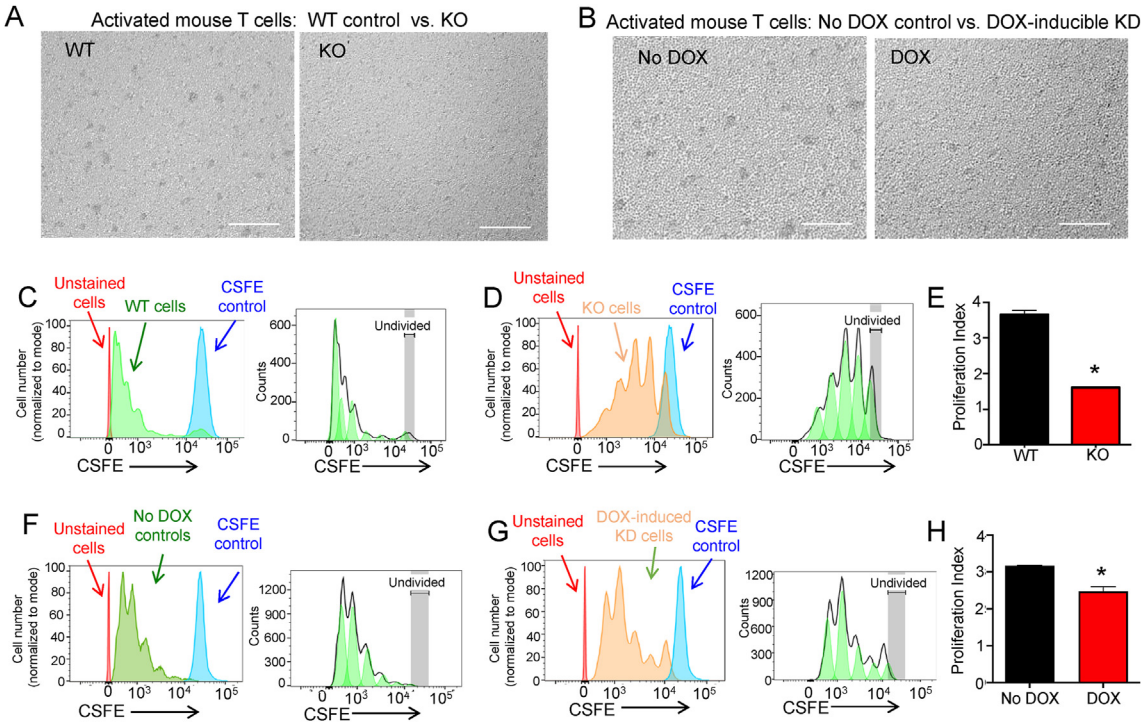

Figure 3: SELENOI deficiency decreased T cell proliferation. (A) WT and SELENOI KO T cells or (B) No DOX control and DOX-induced SELENOI KD T cells were visualized after 18 h of activation for density of proliferating clusters. KO and KD T cells exhibited fewer clusters. Scale bar = 125 mm. (C–E) WT and SELENOI KO T cells were loaded with CSFE and its decreasing fluorescent intensity with each round of cell division was measured by flow cytometry, which allowed cell numbers in each cell division group to be determined. After 3 d of activation, T cells were analyzed for the Proliferation Index as described in the Methods section. (F–H) CSFE stained No DOX controls or DOX-induced SELENOI KD T cells were analyzed for proliferation after 3 d of activation. Means of replicates (N = 4) were compared using Student's t test and expressed as mean ± SEM with *p < 0.05.

3.4. SELENOI deficiency did not affect TCR signaling, but decreased the phosphorylation of AMPK during later stages of T cell activation

Weak TCR signals can impair proliferative capacity, and previous research suggested that the extreme loss of plasmenyl PE in innate immune cells can weaken receptor-mediated signaling initiated at the plasma membrane [38,39]. We then evaluated the effects of SELENOI deficiency on TCR-induced signaling. When the SELENOI KO T cells were compared to the WT controls, no differences in TCR-induced phosphorylation of key signaling molecules ERK or AKT were detected (Figure 5A–C). TCR-induced signaling converged downstream to increase the transcription of growth factor IL-2 and the high affinity chain of IL-2R, CD25, and levels of those transcripts were not diminished by SELENOI deficiency (Figure 5D–E).

Although early TCR signaling was not directly affected by the SELENOI KO, these signaling networks may be modulated at later stages through feedback mechanisms such as those involving the metabolite sensors mTORC2 and AMPK. For example, mTORC2 has been shown to respond to growth factors by its activation through phosphorylation of Thr1135 on the Rictor subunit protein that in turn modulates cell metabolism and proliferation [40]. Phosphorylation of AMPK at Thr172 is also required for its activation to promote full activation [41]. A time-course assay showed that the WT and SELENOI KO T cells exhibited similar levels of p-Rictor at 1, 3, and 5 h post-TCR stimulation (Figure 5F). Levels of p-AMPK (p-Thr172) at early time points of 1 and 3 h post-TCR stimulation did not differ between the WT and SELENOI KO T cells, but the KO T cells exhibited lower levels of p-AMPK at 5 h post-TCR stimulation. Repeat experiments were conducted at the 5 h time point and densitometry for all three blots demonstrated >50% decreased p-AMPK, but no changes in p-Rictor in the SELENOI KO T cells (Figure 5G–H).

The previously described data showing increased p-AMPK over 5 h post-TCR stimulation in the WT T cells suggest that maintaining elevated phosphorylation and activation of AMPK may be important for proliferation, which is consistent with our data showing less p-AMPK and reduced proliferation in our KO T cells. To determine whether restraining the TCR-induced increase in p-AMPK was sufficient to cause reduced proliferation, we activated T cells in the presence of a specific inhibitor of AMPK phosphorylation, dorsomorphin, at increasing concentrations and measured the proliferation (Figure 6A–B). The results showed that increasing concentrations of dorsomorphin led to decreasing cellular proliferation (Figure 6C), with a 0.75 mM concentration of dorsomorphin most similar in its ability to inhibit the Proliferation Index compared to SELENOI. Consistent with this finding, the 0.75 mM concentration of dorsomorphin reduced the phosphorylation of AMPK by levels similar to SELENOI KO (Figure 6D). These results using dorsomorphin suggest that the effects of SELENOI deficiency on lowering p-AMPK levels by > 50% were sufficient to decrease the proliferative capacity of activated T cells. These results also suggest that SELENOI deficiency during TCR-induced activation may lead to excess ATP given that high [ATP] is a negative regulator of AMPK phosphorylation, which led us to investigate ATP accumulation and metabolic pathways.

3.5. SELENOI deficiency caused ATP accumulation and disrupted metabolism

Energy production during TCR-induced activation was monitored in live SELENOI KO T cells and WT controls by evaluating real-time glycolysis

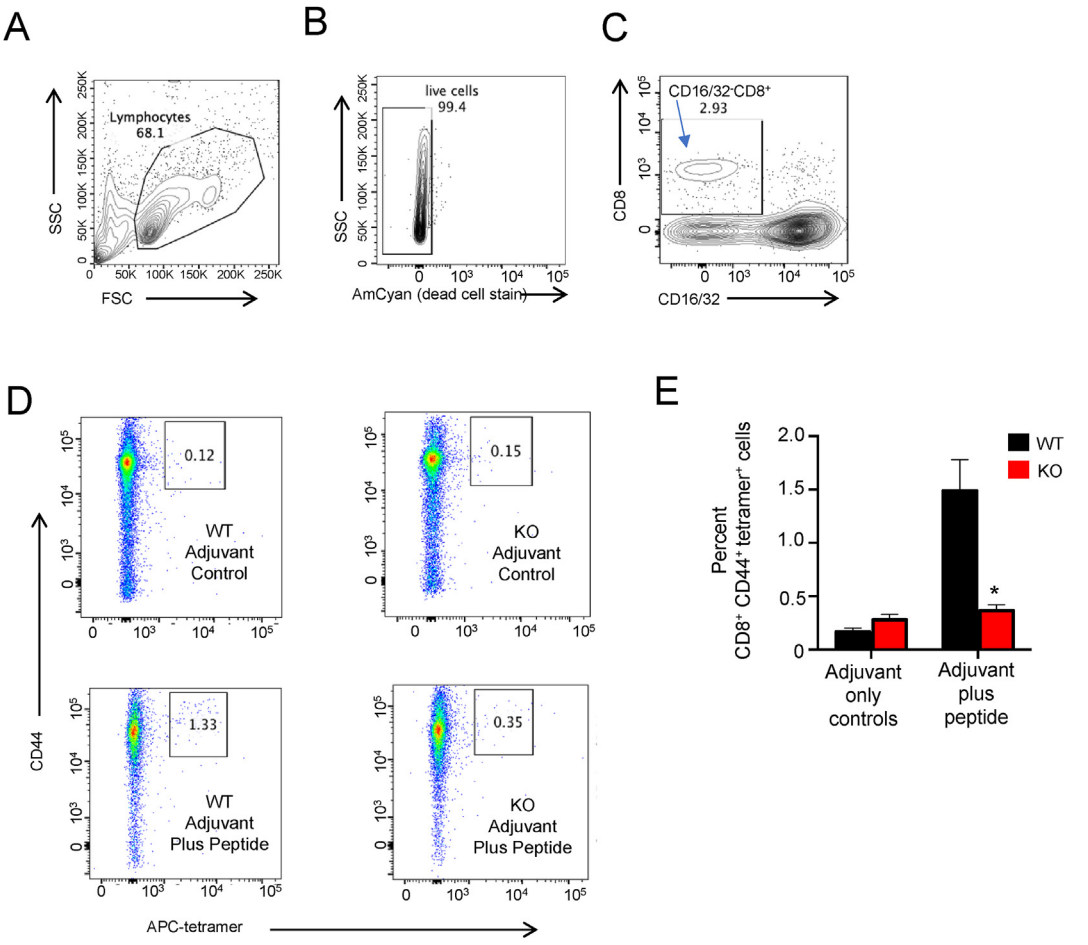

Figure 4: In vivo antigen challenge demonstrated decreased proliferation in SELENOI KO T cells. Spleen cells from LCMV gp33-41 vaccinated mice were analyzed by flow cytometry using the H-2D^{b}-KAVYNFATM-APC tetramer. (A–C) The gating strategy is shown in which single cells were analyzed for lymphocytes excluding debris that were gated for live cells that were then analyzed for CD16/32^{-}CD8^{+} non-phagocytic T cells. (D) The latter cells were analyzed for percent antigen experienced CD44^{+}tetramer^{+} T cells. Representative dot plots of samples from WT and KO mice injected with adjuvant alone or adjuvant plus LCMV gp33-41 peptide are shown. (E) The results showed that KO mice generated lower levels of antigen-specific T cells compared to WT controls. Means of replicates (n = 4 mice/group) were compared using Student's t test and expressed as mean ± SEM with *p < 0.05.

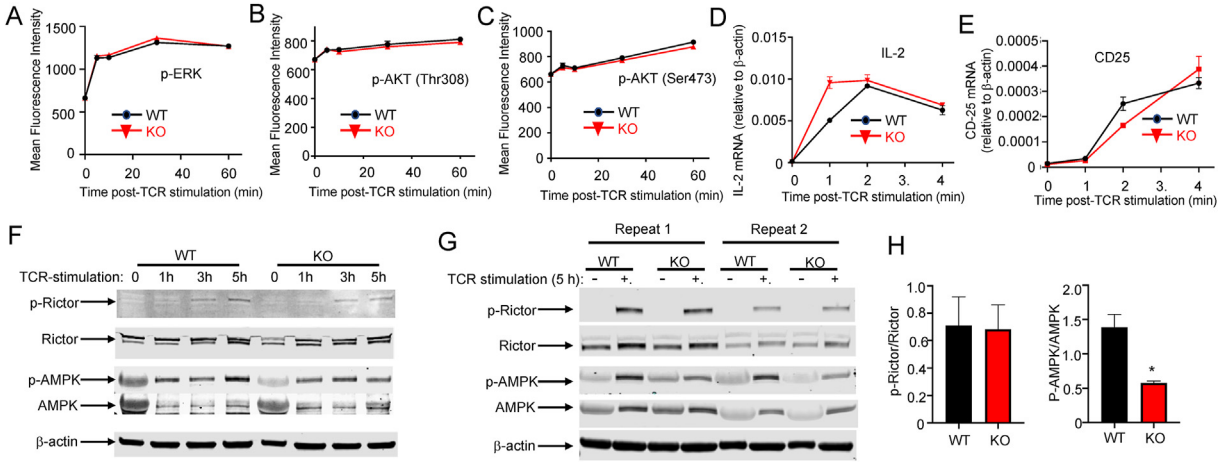

Figure 5: SELENOI deficiency did not impact TCR signal strength, but led to reduced activation of metabolic-sensing protein AMPK. A time-course analyses (0–1 h) of TCR-induced activation of (A) ERK and (B–C) AKT showed no differences between WT and SELENOI KO T cells using flow cytometry. Real-time PCR was used to evaluate gene transcription downstream of TCR signaling including (D) IL-2 mRNA and (E) CD25 mRNA, with β-actin used as a housekeeping transcript for both. (F) Western blotting analyses of p-Rictor/Rictor and p-AMPK/AMPK from 0 to 5 h post-TCR activation of WT and SELENOI KO T cells. (G–H) Two repeat western blotting experiments at the 5 h time point and densitometry on three sets of results showed that SELENOI KO T cells had less phosphorylation of AMPK, but phosphorylation of Rictor was similar to WT. Means of replicates (n = 4 for A–E; n = 3 for H) were compared using Student's t test. Data represent mean ± SEM with *p < 0.05.

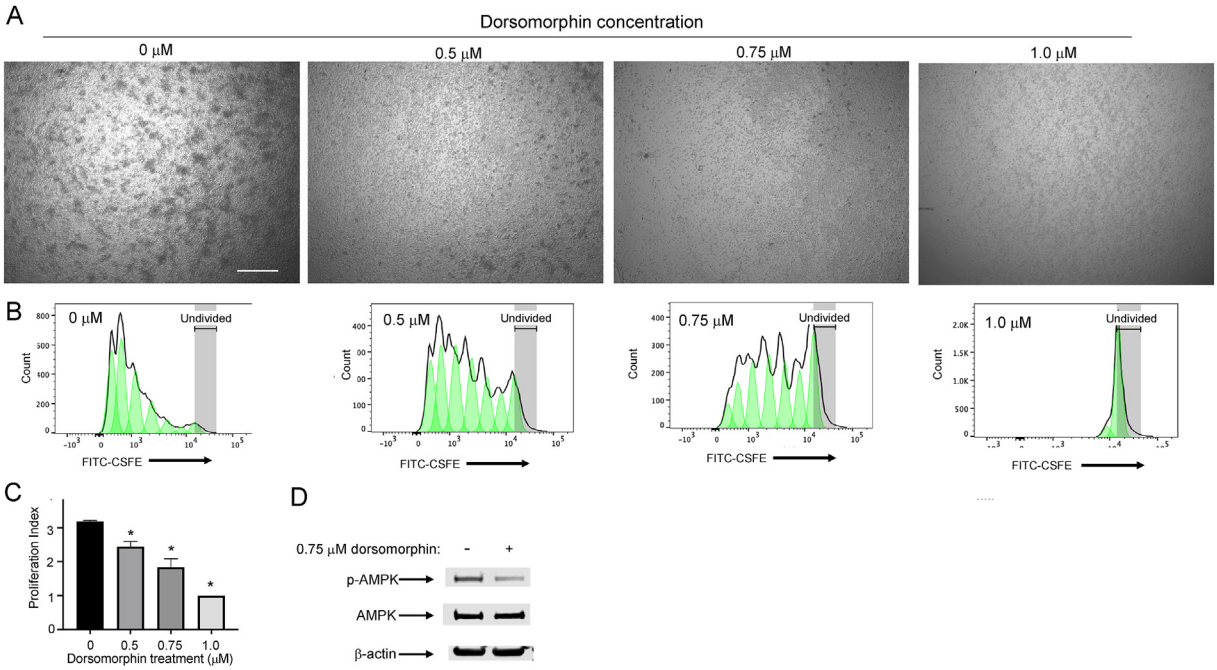

Figure 6: Dorsomorphin treatment inhibited T cell proliferation. Activated WT T cells were treated with different doses of dorsomorphin during CSFE assays. (A) Images of cultured cells at 18 h post-TCR-stimulation with clusters of proliferating cells decreasing with increasing doses of dorsomorphin. Scale bar = 125 mm. (B) Flow cytometry data used to calculate the Proliferation Index. (C) CSFE assays using different concentrations of the AMPK inhibitor, dorsomorphin, decreased the Proliferation Index from the data shown in Figure S5. (D) Western blot analysis showed that 0.75 mM of dorsomorphin treatment led to decreased phosphorylation of AMPK after 5 h of TCR stimulation similar to SELENOI KO. Means of replicates (n = 3) were compared using Student's t test and means in panel I (n = 4) were analyzed using one-way ANOVA with Tukey's post-test and expressed as mean ± SEM with *p < 0.05.

and mitochondrial respiration. For 30 min following TCR stimulation, increased glycolysis (a major component of metabolic reprograming) was observed as expected in the WT T cells with a slower increase found in the SELENOI KO T cells (Figure 7A), although no statistical differences were found at individual time points. Mitochondrial respiration was similar between the two groups (Figure 7B). The reduced glycolytic rate during 30 min was consistent with slightly lower ATP levels observed in the SELENOI KO T cells at 30 min post-TCR stimulation (Figure 7C). Interestingly, from 1 to 6 h post-TCR stimulation, the ATP levels accumulated at higher levels in the SELENOI KO T cells compared to the controls. This was consistent with the previously described data showing lower p-AMPK at 5 h post-TCR stimulation since high [ATP] causes reduced phosphorylation AMPK.

The ATP accumulation in the SELENOI KO T cells 1–7 h after TCR stimulation as previously reported suggests that metabolic reprograming may be disrupted during this critical period as the cells balance catabolic/anabolic pathways in preparation for mitosis. Thus, we chose the 5 h time point to perform metabolomic analyses on the SELENOI KO T cells and WT controls. Interestingly, minimal changes in cellular glucose levels were observed between the KO and WT T cells (Figure 7D). Consistent with the lower glycolytic rate previously described for the SELENOI KO T cells, decreases in glycolytic intermediates, particularly hexose 1,6-diphosphates, were evident in the KO T cells at 5 h post-activation. A central pentose phosphate pathway (PPP) intermediate, sedoheptulose-7-phosphate, was significantly increased in the KO cells, suggesting increased diversion of glucose carbon from glycolysis into the PPP. Nucleotide metabolism was dramatically altered in the SELENOI KO T cells, with elevated levels of several metabolites including inosine 5′-monophosphate (IMP), uracil, xanthine, cytidine, and thymidine (Figure 7E). This may reflect disruptions in energy-preserving salvage reactions, increased DNA/RNA degradation, or increased PPP. An expanded list of metabolites detected by the analyses of the WT and SELENOI KO T cells activated for 5 h are included in Table S1, and it is important to note that, as expected, CDP-ethanolamine (substrate for SELENOI) significantly increased by 1.36-fold in the SELENOI KO T cells 5 h post-activation.

3.6. SELENOI deficiency altered transcriptional programs involving decreased cell cycle factors and glycosylphosphatidylinositol (GPI) anchor synthesis/attachment

To better understand the outcome of SELENOI deficiency in activated T cells, we assessed transcriptomic differences between the activated SELENOI WT and KO T cells at 18 h post-TCR stimulation using unbiased gene array assays. The results showed the detection of differentially expressed genes (DEGs) with a majority exhibiting downregulation in the SELENOI KO T cells compared to the controls (Figure S5). Integrated pathway analyses revealed that, after 18 h of TCR-induced activation, there were substantial decreases in several pro-growth pathways including cell cycle progression, energy production, DNA replication, and purine metabolism. Real-time PCR was performed to confirm that the SELENOI KO led to decreased mRNA levels for 3 important cell cycle promoting factors: budding uninhibited by benzimidazoles 1 (BUB1), cyclin E1 (CCNE1), and E2F transcription factor 3 (E2F3). Consistent with the previously described metabolomics data, these results demonstrated that SELENOI deficiency in activated T cells disrupted several pathways with purine synthesis and DNA replication particularly affected, culminating in impaired cell cycle progression and reduced proliferation.

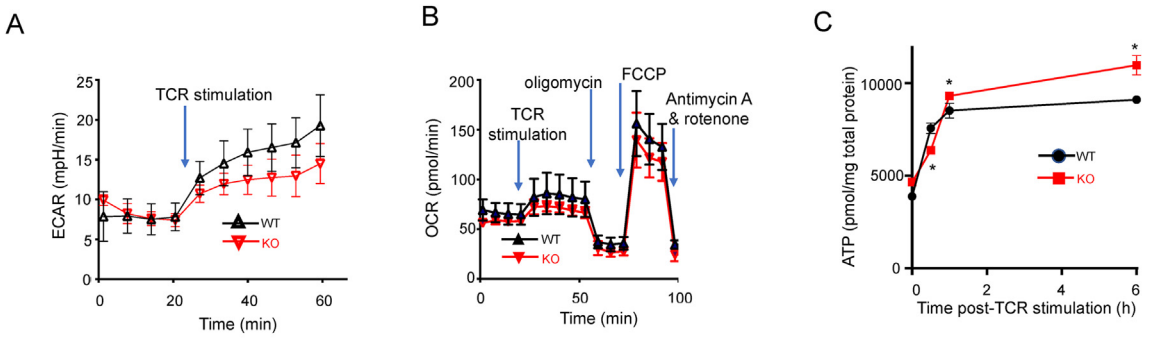

D

	Metabolite	KO T cells / WT T cells	p-value
Glycolysis	glucose	0.90	0.6817
	fructose 1,6-diphosphate glucose 1,6-diphosphate myo-inositol diphosphates	0.55	0.0013
	dihydroxyacetone phosphate (DHAP)	0.83	0.0982
	3-phosphoglycerate	0.69	0.1294
	phosphoenolpyruvate (PEP)	0.68	0.0838
	pyruvate	1.11	0.4357
	lactate	1.00	0.8470
Pentose Phosphate Pathway	6-phosphogluconate	0.66	0.0704
	sedoheptulose-7-phosphate	1.57	0.0206

E

	Metabolite	KO T cells / WT T cells	p-value
Purine Metabolism	inosine 5'-monophosphate (IMP)	1.58	0.0115
	xanthine	1.38	0.0194
	xanthosine	0.97	0.9455
	urate	0.83	0.2498
	adenosine 5'-monophosphate (AMP)	1.11	0.3775
	adenosine 2'-monophosphate (2'-AMP)	1.61	0.0667
	adenine	1.38	0.0609
	N1-methyladenosine	1.49	0.0462
	guanosine 5'-diphosphate (GDP)	0.59	0.0482
	guanosine 5'-monophosphate (5'-GMP)	1.28	0.0368
	guanine	1.23	0.1488
Pyrimidine Metabolism	uridine 5'-triphosphate (UTP)	0.38	0.0123
	uridine 5'-diphosphate (UDP)	0.66	0.0576
	uracil	1.63	0.0012
	cytidine triphosphate	0.42	0.0393
	cytidine	1.47	0.0161
	2'-deoxycytidine 5'-monophosphate	1.49	0.0099
	thymidine	1.38	0.0462

Figure 7: Activated SELENOI KO T cells exhibited reduced glycolysis and disrupted biosynthetic pathways along with ATP accumulation. (A) Glycolysis was evaluated in live cells by measuring the extracellular acidification rate (ECAR) using an Agilent Seahorse instrument. After a baseline reading, anti-CD3/CD28-coated beads were introduced to activate T cells. (B) Mitochondrial energy production was simultaneously evaluated by measuring the oxygen consumption rate (OCR). Oligomycin was used to inhibit ATP synthase (complex V), FCCP to disrupt mitochondrial membrane potential causing uninhibited flow through the ETC that maximizes oxygen consumption by complex IV, and rotenone (complex I inhibitor) with antimycin A (complex III inhibitor) that enable the measurement of non-mitochondrial respiration. (C) ATP was measured using a bioluminescence assay over an activation time-course using WT and SELENOI KO T cells. (D–E) Metabolite analyses for glycolysis/PPP and purine/pyrimidine metabolism along with a statistical heat map at 5 h post-activation. Trending ($p = 0.05 < 0.10$) and significant ($p \leq 0.05$) elevations are indicated by pink and red with bolded text, respectively, while trending and significant reductions are represented by light green and dark green with bolded text, respectively. Means of replicates ($n = 4$/group for A–C) were compared using Student's t test; and means in E ($n = 8$/group) were analyzed using Welch's two-sample t test.

One important DEG identified by this experiment was that encoding glycosylphosphatidylinositol (GPI) anchored attachment protein 1 (GPAA1), an enzyme that post-translationally transfers GPI anchors to ~150 proteins to tether these GPI-anchored proteins to plasma membranes [42]. Real-time PCR and western blotting confirmed lower levels of GPAA1 in the activated SELENOI KO T cells compared to the WT controls (Figure 8A–C). As PE is used as a source of ethanolamine in the synthesis of GPI anchors [43], the decreased de novo PE synthesis and downregulated GPAA1 in the SELENOI KO T cells may have led to lower levels of GPI-anchored proteins on the plasma membrane surface. To investigate this possibility, flow cytometry was used to measure the levels of 8 different GPI-anchored proteins over 3 days after TCR-induced activation. The results showed that the SELENOI KO led to decreased surface levels in 5 of the 8 GPI-anchored proteins: CD52, CD90, CD73, CD109, and CD44 (Figure 8D), suggesting an important role of SELENOI-dependent ethanolamine phospholipid synthesis for maintaining the GPI anchor synthesis/attachment pathway for some but not all GPI-anchored proteins.

4. DISCUSSION

SELENOI is a versatile enzyme participating in two phospholipid synthesis pathways: it may transfer the ethanolamine headgroup from CDP-ethanolamine to either DAG or AAG to generate PE or plasmenyl PE, respectively. Although SELENOI participates in the biosynthesis of both, data from HeLa and HEK293 cell lines suggested that, in the absence of SELENOI, mainly plasmenyl PE levels are reduced since cells can utilize choline/ethanolamine phosphotransferase 1 (CEPT1) to maintain PE synthesis [34,35]. Our results suggest that the same is true for T cells as only plasmenyl PE in the labeled and unlabeled forms were lower in the SELENOI KO T cells. During T cell activation, both PE and plasmenyl PE synthesis ($^{13}C_2$-labeled forms) were impaired in the SELENOI KO T cells, with de novo plasmenyl PE being particularly dependent on SELENOI. Neither PE nor plasmenyl PE were completely eliminated by the SELENOI KO, suggesting that T cells likely have some capacity to complete both synthesis pathways in the absence of SELENOI and this may be through CEPT1 activity or conversion of other phospholipids. In fact, little is known regarding the activity of CEPT1, its regulation during T cell activation, or its ability to compensate for the loss of SELENOI activity in T cells. Regardless, the functional consequences of lowering de novo synthesis of PE by ~23% and plasmenyl PE by ~64% in the activated KO T cells were substantial, reducing ex vivo proliferation by ~56% and in vivo proliferation by ~75%. These data highlight the importance of increased PE and plasmenyl PE synthesis by upregulated SELENOI activity in T cells during activation and its requirement for effective proliferation.

The role of SELENOI-dependent synthesis pathways in T cells is of particular interest given that "phospholipid remodeling" has recently emerged as a potential regulator of cell fate decisions [10,11]. Our results showed that increased SELENOI may be part of the phospholipid remodeling process in activated T cells. Without increased SELENOI available during T cell activation, there is a decrease in the

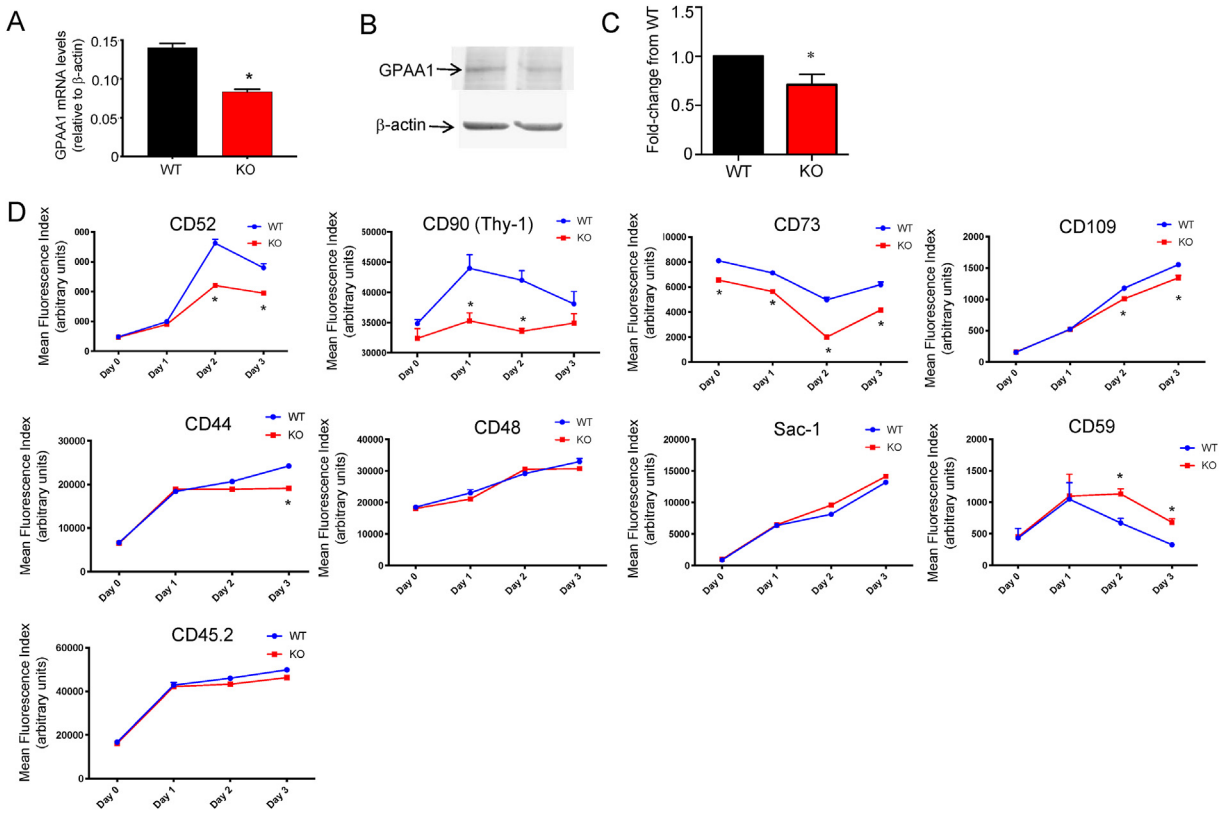

Figure 8: The GPI anchor synthesis/attachment pathway was disrupted in SELENOI KO T cells. (A) Real-time PCR showed that relative mRNA levels for GPAA1 decreased in SELENOI KO T cells compared to WT controls after 18 h of activation. (B–C) Representative Western blotting and densitometry analysis of GPAA1 protein levels from 3 replicate experiments showed lower levels in SELENOI KO T cells after 18 h of activation, and β-actin was used as a loading control. (D) Flow cytometry was used to measure cell surface levels of a panel of 8 GPI-anchored proteins prior to and 1–3 days after TCR stimulation. CD45.2 was included as a non-GPI-anchored protein control. Means of replicates ($n = 3$) were compared using Student's t test and expressed as mean + SEM with $^*p < 0.05$.

two anabolic phospholipid pathways in which it participates, de novo PE and plasmenyl PE synthesis. This causes a cascade of effects including a disruption of energy and metabolite producing pathways and accumulation of ATP that is sensed by AMPK that is hypo-phosphorylated in SELENOI-deficient T cells. It was not determined whether the net effect of altered metabolic pathways directly caused the ATP accumulation in the KO T cells, but the lower p-AMPK and ATP accumulation during activation in the SELENOI KO T cells suggested a cause–effect relationship between loss of SELENOI activity and inef-fective utilization of ATP. In this sense, AMPK phosphorylation may represent a checkpoint for ensuring intact, properly functioning phospholipid reprogramming during T cell activation before proceeding to cell cycling. A rescue experiment involving the addition of PE and/or plasmenyl PE to SELENOI KO T cells would clarify the causative role of these phospholipids in optimal AMPK phosphorylation during T cell activation. Unfortunately, these lipid reagents added exogenously are incorporated into the plasma membrane and would therefore not restore ethanolamine phospholipids generated by SELENOI in the ER, but other experimental approaches are currently being explored. AMPK is a critical sensor of the inefficient use of ATP [44], and SELENOI deficiency leading to lower p-AMPK may reflect an attempt by these cells to slow cell proliferation until balanced ATP-consuming/generating pathways may be restored.

Importantly, AMPK is not just a sensor, but it also acts as an effector protein that is tightly regulated in terms of its activation levels and downstream actions [45]. While hyperactivation of AMPK may inhibit anabolic pathways such as protein and fatty acid synthesis, hypo-activation of AMPK may also interfere with the metabolic plasticity required to promote cell cycle progression [8]. The latter was sup-ported by our experiments involving treating T cells with the specific inhibitor of AMPK, dorsomorphin. In particular, treating the WT T cells with this drug at the 0.75 mM concentration that reduced AMPK at 5 h post-TCR stimulation by ~50% similar to the SELENOI KO caused a reduction in proliferation after 3 d similar to the SELENOI KO. Ulti-mately, the disrupted metabolic pathways in the SELENOI KO T cells led to restricted expression of several factors critical for cell cycle progression and proliferation as demonstrated by our analyses of DEGs. Exactly how reduced PE and plasmenyl PE synthesis interrupts metabolic pathways is most likely multifactorial and complex. Our Seahorse-based analyses of TCR-induced energy production sug-gested that lower glycolytic rates in SELENOI KO T cells may be an early contributor to metabolic deficiencies. This was supported by the metabolomic analyses at 5 h post-activation. As a major component of metabolic reprogramming in activated T cells, increased glycolysis is critical for generating intermediate metabolites that feed into anabolic pathways [6,46]. Thus, lower glycolytic rates that lead to reduced precursors for biosynthetic pathways during the early stages of TCR-induced activation may be difficult to overcome, and the cells may overcompensate through increased PPP or DNA/RNA degradation. This idea was supported by our metabolomics data, and the gene array data showed a variety of pro-proliferative pathways that were down-regulated in the SELENOI KO T cells at 18 h post-stimulation.

Upon TCR activation, T cells experience increased demands required for cellular proliferation [47]. TCR activation induces de novo synthesis of proteins, nucleic acids, and fatty acids accompanied by a doubling of cell sizes [30,48]. These processes are critical for subsequent cell division and clonal expansion that drive effective immune responses. IL-2 production occurs downstream of TCR engagement and acts in an autocrine and paracrine manner to stimulate T cell proliferation through a cascade of cytoplasmic signaling and culminates in pro-growth transcriptional programs. Increased SELENOI appears to be an important part of TCR-triggered changes occurring in activated T cells, although the specific role of IL-2-dependent signaling in upregulating SELENOI was not determined in this study. Interestingly, neither cell size nor early TCR-induced signaling were affected by SELENOI KO, suggesting no major defects in the T cell plasma membrane structure or dynamics. In a previous study using the plasmenyl PE-deficient mouse macrophage cell line, RAW.108, defects in plasma membrane raft density, membrane fluidity, and zymosan-induced signaling were detected [39]. This cell line was shown to have a mutation leading to impaired D1′-desaturase activity that is upstream of SELENOI in the plasmenyl PE synthesis pathway [49]. The plasmenyl PE content in these cells was negligible, much lower than our SELENOI KO T cells. This suggests that an intermediate deficiency in plasmenyl PE (SELENOI KO) may impair metabolism in T cells while leaving plasma membrane signaling intact, but mutations that lower plasmenyl PE to negligible levels (D1′-desaturase mutation) may impact plasma membrane structure and signaling and perhaps also compromise cellular metabolism.

5. CONCLUSIONS

Overall, our data revealed that SELENOI-dependent PE and plasmenyl PE synthesis increased upon T cell activation as crucial contributors to cell cycle progression. Increased production of these ethanolamine phospholipids is an important part of the dramatic changes in cellular metabolism induced by TCR stimulation, promoting balanced biomolecule synthesis and energy production for cellular proliferation. ATP accumulation and decreased AMPK activation result from disrupted SELENOI activity, and lower phosphorylation at Thr172 of AMPK is sufficient to inhibit proliferation as demonstrated by our experiments using dorsomorphin treatment. SELENOI is also required to maintain the GPI anchor synthesis/attachment pathway. We found that 5 of 8 GPI-anchored proteins were lower in the activated SELENOI KO T cells, which may reflect surface-linked proteins with higher turnover or those that are more dependent on high pools of GPI anchors and/or GPAA1 activity. Altogether, these findings provide insight into the response of these phospholipid synthesis pathways and their contribution to metabolic reprogramming that is critical for T cell proliferation and optimal immunity.

AUTHOR CONTRIBUTIONS

C.M., F.W.H., F.D.H., and P.R.H. conceived, designed, and supervised the experiments. M.G., J.U., S.M., and Y.D. were responsible for the core facilities involved in this study. S.R. provided key reagents for this study. C.M., F.W.H., M.P.M., K.E.P., M.A.W.-A., G.S.G, J.U., and V.S.K. conducted the experiments. F.D.H. and P.R.H. interpreted the data. P.R.H. wrote the manuscript. All of the authors read and approved the final manuscript. We thank Grant Hogg, Olivia Honaker, and Nigel Hataye for technical assistance.

ACKNOWLEDGMENTS

This research was supported by NIH grants R01AI147496, P20GM103466, P20GM113134, P30GM131944, and P30GM114737, and the reagents were supplied by the NIH Tetramer Core Facility. This study was also supported by the Genomics and Bioinformatics Shared Resource (GBSR, RRID: SCR_019085) at UHCC that is supported by NCI 5P30CA071789.

CONFLICT OF INTEREST

None declared.

APPENDIX A. SUPPLEMENTARY DATA

Supplementary data to this article can be found online at https://doi.org/10.1016/j.molmet.2021.101170.

REFERENCES

[1] Jones, R.G., Thompson, C.B., 2007. Revving the engine: signal transduction fuels T cell activation. Immunity 27(2):173–178.
[2] Bayer, A.L., Pugliese, A., Malek, T.R., 2013. The IL-2/IL-2R system: from basic science to therapeutic applications to enhance immune regulation. Immunologic Research 57(1–3):197–209.
[3] Bhattacharyya, N.D., Feng, C.G., 2020. Regulation of T Helper cell fate by TCR signal strength. Frontiers in Immunology 11:624.
[4] Croft, M., Dubey, C., 2017. Accessory molecule and costimulation requirements for CD4 T cell response. Critical Reviews in Immunology 37(2–6): 261–290.
[5] Almeida, L., Lochner, M., Berod, L., Sparwasser, T., 2016. Metabolic pathways in T cell activation and lineage differentiation. Seminars in Immunology 28(5): 514–524.
[6] MacIver, N.J., Michalek, R.D., Rathmell, J.C., 2013. Metabolic regulation of T lymphocytes. Annual Review of Immunology 31:259–283.
[7] Ma, E.H., Poffenberger, M.C., Wong, A.H., Jones, R.G., 2017. The role of AMPK in T cell metabolism and function. Current Opinion in Immunology 46:45–52.
[8] Hardie, D.G., Ross, F.A., Hawley, S.A., 2012. AMPK: a nutrient and energy sensor that maintains energy homeostasis. Nature Reviews Molecular Cell Biology 13(4):251–262.
[9] Wang, R., Green, D.R., 2012. Metabolic checkpoints in activated T cells. Nature Immunology 13(10):907–915.
[10] Wu, Y., Chen, K., Xing, G., Li, L., Ma, B., Hu, Z., et al., 2019. Phospholipid remodeling is critical for stem cell pluripotency by facilitating mesenchymal-to-epithelial transition. Science Advances 5(11):eaax7525.
[11] Wang, B., Rong, X., Palladino, E.N.D., Wang, J., Fogelman, A.M., Martin, M.G., et al., 2018. Phospholipid remodeling and cholesterol availability regulate intestinal stemness and tumorigenesis. Cell Stem Cell 22(2):206–220 e204.
[12] Reeves, M.A., Hoffmann, P.R., 2009. The human selenoproteome: recent insights into functions and regulation. Cellular and Molecular Life Sciences 66(15):2457–2478.
[13] Horibata, Y., Hirabayashi, Y., 2007. Identification and characterization of human ethanolaminephosphotransferase1. The Journal of Lipid Research 48(3): 503–508.
[14] Vance, J.E., 2018. Historical perspective: phosphatidylserine and phosphatidylethanolamine from the 1800s to the present. The Journal of Lipid Research 59(6):923–944.
[15] Gibellini, F., Smith, T.K., 2010. The Kennedy pathway–De novo synthesis of phosphatidylethanolamine and phosphatidylcholine. IUBMB Life 62(6):414–428.

[16] Braverman, N.E., Moser, A.B., 2012. Functions of plasmalogen lipids in health and disease. Biochimica et Biophysica Acta 1822(9):1442—1452.
[17] Lebrero, P., Astudillo, A.M., Rubio, J.M., Fernandez-Caballero, L., Kokotos, G., Balboa, M.A., et al., 2019. Cellular plasmalogen content does not influence arachidonic acid levels or distribution in macrophages: a role for cytosolic phospholipase A2gamma in phospholipid remodeling. Cells 8(8).
[18] Avery, J.C., Yamazaki, Y., Hoffmann, F.W., Folgelgren, B., Hoffmann, P.R., 2020. Selenoprotein I is essential for murine embryogenesis. Archives of Biochemistry and Biophysics 689:108444.
[19] Zhang, D.J., Wang, Q., Wei, J., Baimukanova, G., Buchholz, F., Stewart, A.F., et al., 2005. Selective expression of the Cre recombinase in late-stage thymocytes using the distal promoter of the Lck gene. The Journal of Immunology 174(11):6725—6731.
[20] Urschitz, J., Kawasumi, M., Owens, J., Morozumi, K., Yamashiro, H., Stoytchev, I., et al., 2010. Helper-independent piggyBac plasmids for gene delivery approaches: strategies for avoiding potential genotoxic effects. Proceedings of the National Academy of Sciences of the USA 107(18):8117—8122.
[21] Marh, J., Stoytcheva, Z., Urschitz, J., Sugawara, A., Yamashiro, H., Owens, J.B., et al., 2012. Hyperactive self-inactivating piggyBac for transposase-enhanced pronuclear microinjection transgenesis. Proceedings of the National Academy of Sciences of the USA 109(47):19184—19189.
[22] Hoffmann, P.R., Hoffmann, F.W., Premeaux, T.A., Fujita, T., Soprana, E., Panigada, M., et al., 2019. Multi-antigen vaccination with simultaneous engagement of the OX40 receptor delays malignant mesothelioma growth and increases survival in animal models. Frontiers in Oncology 9:720.
[23] Verma, S., Hoffmann, F.W., Kumar, M., Huang, Z., Roe, K., Nguyen-Wu, E., et al., 2011. Selenoprotein K knockout mice exhibit deficient calcium flux in immune cells and impaired immune responses. The Journal of Immunology 186(4):2127—2137.
[24] Hoffmann, P.R., Hoge, S.C., Li, P.A., Hoffmann, F.W., Hashimoto, A.C., Berry, M.J., 2007. The selenoproteome exhibits widely varying, tissue-specific dependence on selenoprotein P for selenium supply. Nucleic Acids Research 35(12):3963—3973.
[25] Hoffmann, F.W., Hashimoto, A.C., Shafer, L.A., Dow, S., Berry, M.J., Hoffmann, P.R., 2010. Dietary selenium modulates activation and differentiation of CD4+ T cells in mice through a mechanism involving cellular free thiols. Journal of Nutrition 140(6):1155—1161.
[26] Folch, J., Lees, M., Sloane Stanley, G.H., 1957. A simple method for the isolation and purification of total lipides from animal tissues. Journal of Biological Chemistry 226(1):497—509.
[27] Matyash, V., Liebisch, G., Kurzchalia, T.V., Shevchenko, A., Schwudke, D., 2008. Lipid extraction by methyl-tert-butyl ether for high-throughput lipidomics. The Journal of Lipid Research 49(5):1137—1146.
[28] Ulmer, C.Z., Yost, R.A., Chen, J., Mathews, C.E., Garrett, T.J., 2015. Liquid chromatography-mass spectrometry metabolic and lipidomic sample preparation workflow for suspension-cultured mammalian cells using Jurkat T lymphocyte cells. Journal of Proteomics & Bioinformatics 8(6):126—132.
[29] Takemoto, J.K., Miller, T.L., Wang, J., Jacobson, D.L., Geffner, M.E., Van Dyke, R.B., et al., 2017. Insulin resistance in HIV-infected youth is associated with decreased mitochondrial respiration. AIDS 31(1):15—23.
[30] Teague, T.K., Munn, L., Zygourakis, K., McIntyre, B.W., 1993. Analysis of lymphocyte activation and proliferation by video microscopy and digital imaging. Cytometry 14(7):772—782.
[31] Hullin-Matsuda, F., Makino, A., Murate, M., Kobayashi, T., 2016. Probing phosphoethanolamine-containing lipids in membranes with duramycin/cinnamycin and aegerolysin proteins. Biochimie 130:81—90.
[32] Calzada, E., Onguka, O., Claypool, S.M., 2016. Phosphatidylethanolamine metabolism in health and disease. International Review of Cell and Molecular Biology 321:29—88.
[33] Lykidis, A., Wang, J., Karim, M.A., Jackowski, S., 2001. Overexpression of a mammalian ethanolamine-specific kinase accelerates the CDP-ethanolamine pathway. Journal of Biological Chemistry 276(3):2174—2179.
[34] Horibata, Y., Ando, H., Sugimoto, H., 2020. Locations and contributions of the phosphotransferases EPT1 and CEPT1 to the biosynthesis of ethanolamine phospholipids. The Journal of Lipid Research.
[35] Horibata, Y., Elpeleg, O., Eran, A., Hirabayashi, Y., Savitzki, D., Tal, G., et al., 2018. EPT1 (selenoprotein I) is critical for the neural development and maintenance of plasmalogen in humans. The Journal of Lipid Research 59(6):1015—1026.
[36] Zumwalde, N.A., Domae, E., Mescher, M.F., Shimizu, Y., 2013. ICAM-1-dependent homotypic aggregates regulate CD8 T cell effector function and differentiation during T cell activation. The Journal of Immunology 191(7):3681—3693.
[37] Adutler-Lieber, S., Friedman, N., Geiger, B., 2018. Expansion and antitumor cytotoxicity of T-cells are augmented by substrate-bound CCL21 and intercellular adhesion molecule 1. Frontiers in Immunology 9:1303.
[38] O'Donnell, V.B., Rossjohn, J., Wakelam, M.J., 2018. Phospholipid signaling in innate immune cells. Journal of Clinical Investigation 128(7):2670—2679.
[39] Rubio, J.M., Astudillo, A.M., Casas, J., Balboa, M.A., Balsinde, J., 2018. Regulation of phagocytosis in macrophages by membrane ethanolamine plasmalogens. Frontiers in Immunology 9:1723.
[40] Hresko, R.C., Mueckler, M., 2005. mTOR.RICTOR is the Ser473 kinase for Akt/protein kinase B in 3T3-L1 adipocytes. Journal of Biological Chemistry 280(49):40406—40416.
[41] Hawley, S.A., Davison, M., Woods, A., Davies, S.P., Beri, R.K., Carling, D., et al., 1996. Characterization of the AMP-activated protein kinase from rat liver and identification of threonine 172 as the major site at which it phosphorylates AMP-activated protein kinase. Journal of Biological Chemistry 271(44):27879—27887.
[42] Kinoshita, T., Ohishi, K., Takeda, J., 1997. GPI-anchor synthesis in mammalian cells: genes, their products, and a deficiency. Journal of Biochemistry 122(2):251—257.
[43] Menon, A.K., Stevens, V.L., 1992. Phosphatidylethanolamine is the donor of the ethanolamine residue linking a glycosylphosphatidylinositol anchor to protein. Journal of Biological Chemistry 267(22):15277—15280.
[44] Lin, S.C., Hardie, D.G., 2018. AMPK: sensing glucose as well as cellular energy status. Cell Metabolism 27(2):299—313.
[45] Tamas, P., Hawley, S.A., Clarke, R.G., Mustard, K.J., Green, K., Hardie, D.G., et al., 2006. Regulation of the energy sensor AMP-activated protein kinase by antigen receptor and Ca2+ in T lymphocytes. Journal of Experimental Medicine 203(7):1665—1670.
[46] Vander Heiden, M.G., Cantley, L.C., Thompson, C.B., 2009. Understanding the Warburg effect: the metabolic requirements of cell proliferation. Science 324(5930):1029—1033.
[47] Lochner, M., Berod, L., Sparwasser, T., 2015. Fatty acid metabolism in the regulation of T cell function. Trends in Immunology 36(2):81—91.
[48] Wang, R., Dillon, C.P., Shi, L.Z., Milasta, S., Carter, R., Finkelstein, D., et al., 2011. The transcription factor Myc controls metabolic reprogramming upon T lymphocyte activation. Immunity 35(6):871—882.
[49] Zoeller, R.A., Rangaswamy, S., Herscovitz, H., Rizzo, W.B., Hajra, A.K., Das, A.K., et al., 1992. Mutants in a macrophage-like cell line are defective in plasmalogen biosynthesis, but contain functional peroxisomes. Journal of Biological Chemistry 267(12):8299—8306.

